Chirality effect on superconductivity

AUTHOR(S):

Morinari, Takao

CITATION:

Morinari, Takao. Chirality effect on superconductivity. Journal of Physics: Conference Series 2015, 603(1)

ISSUE DATE:

2015-04-28

URL:

http://hdl.handle.net/2433/223014

Chirality effect on superconductivity

2015 J. Phys.: Conf. Ser. 603 012007

(http://iopscience.iop.org/1742-6596/603/1/012007)

International Workshop on Dirac Electrons in Solids 2015 IOP Publishing
Journal of Physics: Conference Series **603** (2015) 012007 doi:10.1088/1742-6596/603/1/012007

Chirality effect on superconductivity

Takao Morinari

Graduate School of Human and Environmental Studies, Kyoto University, Kyoto 606-8501, Japan

E-mail: morinari.takao.5s@kyoto-u.ac.jp

Abstract. We consider electron systems characterized by chirality, such as Dirac fermion systems and iron-based superconductors. We investigate the chirality effect on superconducting states in such a system. We show that chirality effect leads to a nodal structure in the superconducting gap function. The node creation mechanism depends on the wave vector $\mathbf{q}$ of the pairing interaction and vorticity that characterizes chirality of electrons. The node creation effect due to chirality is significant for the case of Dirac fermions with $\mathbf{q} = (\pi, 0)$ and for the case of iron-based superconductors with $\mathbf{q} = (\pi, \pi)$.

1. Introduction

Massless Dirac fermions in condensed matter systems have attracted much attention since the discovery of the anomalous integer quantum Hall effect in graphene [1, 2]. In such a Dirac fermion system, the conduction and valence bands touch at a single point. This band structure is called the Dirac cone from its shape and the point of band contact is called the Dirac point. In graphene, the linear energy dispersion exists at the corners of the first Brillouin zone, so that the electrons at low energies are well described by the Dirac equation, with the speed of light being replaced by the Fermi velocity [3]. Physically Dirac fermions and conventional electrons in metals are quite different. For instance, there is qualitative difference in the energy spectrum under magnetic field. For the case of Dirac fermions, the Landau level energies are not equally spaced and the energies depend on the square root of the magnetic field. In particular, there is the zero energy Landau level. The presence of this zero energy Landau level leads to unusual half-integer quantum Hall effect [1, 2].

Another important physical properties of massless Dirac fermions is chirality. There are two types of Dirac fermions: right-handed and left-handed. The Dirac fermion with the wave vector $\mathbf{k}$ is either right-handed, denoted by pseudospin $\uparrow$, or left-handed, denoted by pseudospin $\downarrow$. In the Brillouin zone the pseudospins create a vortex or an anti-vortex configuration at Dirac points. It is well known that the backward scattering is suppressed in Dirac fermion systems because of the chirality effect [4]. In the backward scattering the Dirac fermion state $|\mathbf{k}, \sigma\rangle$ with σ being the pseudospin is scattered into the Dirac fermion state $|-\mathbf{k}, \sigma'\rangle$. Because of the nature of chirality, there is a matrix element for such a scattering process if $\sigma' = \bar{\sigma}$. Namely if the pseudospin is flipped, then there is a matrix element. However, those two energy states have different energies so that there is no matrix elements. The suppression of the backward scattering is understood from the Berry phase argument as well [4]. In addition, there is no Anderson localization. In conventional metals pure two-dimensional systems are insulators because of

the Anderson localization effect. However, reflecting the absence of the Anderson localization, graphene, which is a pure two-dimensional system, is a good conductor.

Electrons in iron-based superconductors are also characterized by chirality. In the antiferromagnetic phase of iron-based superconductors, the Dirac fermion energy spectrum appears near the Fermi energy [5, 6, 7]. It was pointed out that hybridizations between the Fe 3d orbitals and the pnictide ion 4p orbitals give rise to the band degeneracy characterized by a nontrivial topology [5]. Contrary to a conventional spin density wave, there are gapless nodal points along the Fermi surface. The topology here is characterized by vorticity quantum number, which is associated with the phase winding defined through a two component spinor wave function. Although there is no Dirac fermion energy spectrum near the Fermi energy in the absence of the spin-density wave, the electrons in the iron-based superconductors have chirality with vorticity two.

In this paper, we consider superconducting states of electrons characterized by chirality. We study Dirac fermions and electrons with vorticity two. We show that there is a node creation mechanism that is associated with the chirality effect. The nodal structure of the superconducting gap function depends on vorticity. In Sec. 2 we briefly review chirality. In Sec. 3 we study chirality effect on superconducting states of Dirac fermion systems. In Sec. 4 we study chirality effect on superconducting states of iron-based superconductors. We summarize the result in Sec. 5

2. Chirality

In this section we briefly review chirality of Dirac fermions and chirality of electrons in iron-based superconductors.

We first consider Dirac fermion systems. In Dirac fermion systems, there are even number of Dirac points. If there is a Dirac point $\mathbf{k}_D$ in the Brillouin zone, there is another Dirac point at $-\mathbf{k}_D$. If we focus on a single Dirac point, and taking that point as the origin of $\mathbf{k}$ space, the Dirac fermion energy spectrum is described by the following 2×2 Hamiltonian:

$$\mathcal{H} = \hbar v \begin{pmatrix} 0 & k_x - ik_y \\ k_x + ik_y & 0 \end{pmatrix}. \tag{1}$$

Here v is the Fermi velocity. If we rewrite the Hamiltonian as

$$\mathcal{H} = \hbar v \mathbf{k} \cdot \boldsymbol{\sigma}, \tag{2}$$

the right hand side has a form of the Zeeman energy. The psuedospin is denoted by $\boldsymbol{\sigma}$ and $\mathbf{k}$ plays a role of magnetic field. Since $\boldsymbol{\sigma}$ is one-half, if we take the direction of $\mathbf{k}$ as the quantization axis for the pseudospin $\boldsymbol{\sigma}$, the eignestate is either psuedospin $\uparrow$ or $\downarrow$. The state $|\mathbf{k}, \uparrow\rangle$ has the eigen-energy $\varepsilon_k = \hbar v \sqrt{k_x^2 + k_y^2}$ and the state $|\mathbf{k}, \downarrow\rangle$ has the eigen-energy $-\varepsilon_k$.

One can define the vector field

$$\mathbf{n}_\mathbf{k} = \langle \mathbf{k}, \uparrow | \, \boldsymbol{\sigma} \, | \mathbf{k}, \uparrow \rangle \, . \tag{3}$$

For the case of the Hamiltonian above, the vector field $\mathbf{n}_\mathbf{k}$ exhibits radial configuration of pseudospins. The configuration becomes a vortex if we rotate each pseudospin by $\pi/2$ in counterclockwise direction. The Dirac points are represented by such a vortex in the Brillouin zone.

Now let us turn to iron-based superconductors. Iron-based superconductors are a multi-Fermi surface system. All the Fe $3d$ orbitals constitute the Fermi surfaces. There are hole and electron Fermi surfaces with almost equal sizes. Among the Fe $3d$ orbitals d_{xz} and d_{yz} orbitals play an important role. We can take the space of d_{xz} and d_{yz} orbitals as the pseudospin space.

Using the wave function at each point of the Fermi surfaces, we define the pseudospin. Figure 1 shows the pseudospin configuration in the Brillouin zone. As the model Hamiltonian for iron-based superconductors we take a five-band model [8]. We find pseudospins exhibits vortex configurations on each Fermi surface. Contrary to Dirac fermion case, vorticity is not one but two. In fact, the pseudospins on the outer hole Fermi surface at the Γ point rotate twice in clockwise direction when one goes around the Γ point. Similar rotations occur on other Fermi surfaces.

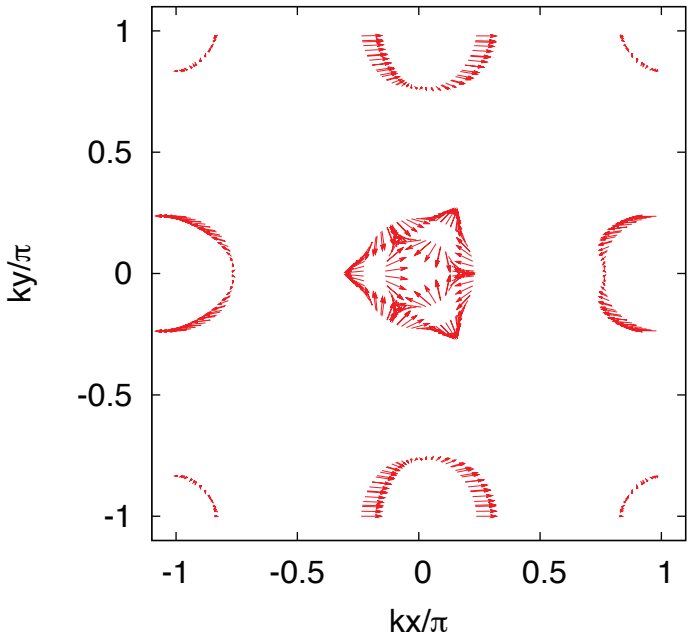

Figure 1. The psuedospin configuration on the Fermi surfaces of iron-based superconductors. The psuedospins on the outer hole Fermi surface at the Γ point rotate twice in clockwise direction when one goes around the Γ point. The psuedospins also rotate twice in either clockwise direction or counterclockwise direction when one goes around $(\pi, 0)$, (π, π), etc.

There are several possibilities of the pseudospin configuration as shown in Fig. 2 which are distinguished by vorticity. Figure 2(a) shows no vorticity case. The Dirac fermion case corresponds to Fig. 2(b). The pseudospins in iron-based superconductors exhibit a vortex configuration as shown in Fig. 2(c). In this case vorticity is two. In the following sections we consider superconducting states of electrons with vorticity.

3. Chirality effect on superconducting states of Dirac fermions

To study superconducting states of electrons characterized by vorticity, we introduce a pairing interaction by hand. We consider the following pairing interaction:

$$V_{\mathbf{k},\mathbf{k}'} = \frac{V_0}{(\mathbf{k} - \mathbf{k}' - \mathbf{q})^2 + \lambda^2}. \tag{4}$$

The scattering wave vector is denoted by $\mathbf{q}$. In the following analysis we consider the $\mathbf{q} = (\pi, 0)$ case and the $\mathbf{q} = (\pi, \pi)$ case. The parameter λ is the interaction range in the Brillouin zone.

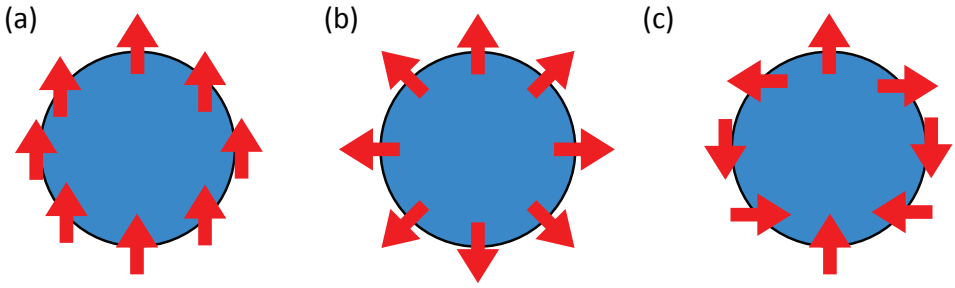

Figure 2. The pseudospin configuration for (a) vorticity zero, (b) vorticity one, and (c) vorticity two. The psudospins are denoted by arrows. The circles represent the Fermi surface.

As the pairing interaction we consider repulsive interactions only. It turns out that there is no significan effect associated with chirality for the case of attractive interactions.

For the analysis of the superconducting state, we solve the linearized BCS gap equation,

$$\Delta_{\mathbf{k}} = \int d\mathbf{k}'_{\parallel} \frac{V_{\mathbf{k},\mathbf{k}'}}{|\mathbf{v}_{\mathbf{k}'}|} \Delta_{\mathbf{k}'}. \tag{5}$$

Here $\Delta_{\mathbf{k}}$ is the gap function. The wave vector $\mathbf{k}$ and $\mathbf{k}'$ are taken those on the Fermi surface. The integral is taken over along the Fermi surface.

Figure 3 shows the result of $\mathbf{q} = (\pi, 0)$ and Fig. 4 shows the result of $\mathbf{q} = (\pi, \pi)$. The Dirac fermion case is Fig. 3(b) and Fig. 4(b) and the normal electron case is Fig. 3(a) and Fig. 4(a). We find that there is a clear qualitative difference for the case of $\mathbf{q} = (\pi, 0)$ between the Dirac fermion case and the normal electron case. The nodal structure is different between the two cases. Because of suppression of the pairing matrix elements due to the chirality effect there is additional nodal structure for the case of Dirac fermions. Contrary, there is no qualitative difference for the case of $\mathbf{q} = (\pi, \pi)$. The gap function has $d_{x^2-y^2}$-wave symmetry but this is just a consequence of the pairing interaction. For the interaction with $\mathbf{q} = (\pi, \pi)$ the chirality effect is not strong but weak. Therefore, there is no significant modification of the gap function.

4. Chirality effect on iron-based superconductors

Now we consider chirality effect on iron-based superconductors. In order to describe the energy band dispersion, we take a five band model with the energy dispersion perpendicular to the Fe-layers [9]. We take the k_x and k_y axises for the two dimensional Fermi surfaces associated with the Fe-layer and the k_z axis for the perpendicular direction. Numerical calculations of the pseudospins, which is defined in Sec. 2, show that the chirality somewhat depends on k_z as shown in Fig. 5. Although there is quantitative difference in the psuedospin configuration for different k_z, the important fact is that vorticity is conserved.

For the analysis of the superconducting gap function, we solve the linearized BCS gap equation as in Sec.3. The gap equation is,

$$\Delta_{\mathbf{k}\alpha} = \sum_{\beta} \int d\mathbf{k}'_{\parallel} \frac{V_{\mathbf{k}\alpha,\mathbf{k}'\beta}}{|\mathbf{v}_{\mathbf{k}'\beta}|} \Delta_{\mathbf{k}'\beta}. \tag{6}$$

Here α and β are indices for the Fermi surfaces.

Figure 6 and Fig. 7 show the result of $\mathbf{q} = (\pi, 0)$ and $\mathbf{q} = (\pi, \pi)$ at $k_z = 0$. The case of iron-based superconductors, which is characterized by vorticity two, is shown in Fig. 6(b) and

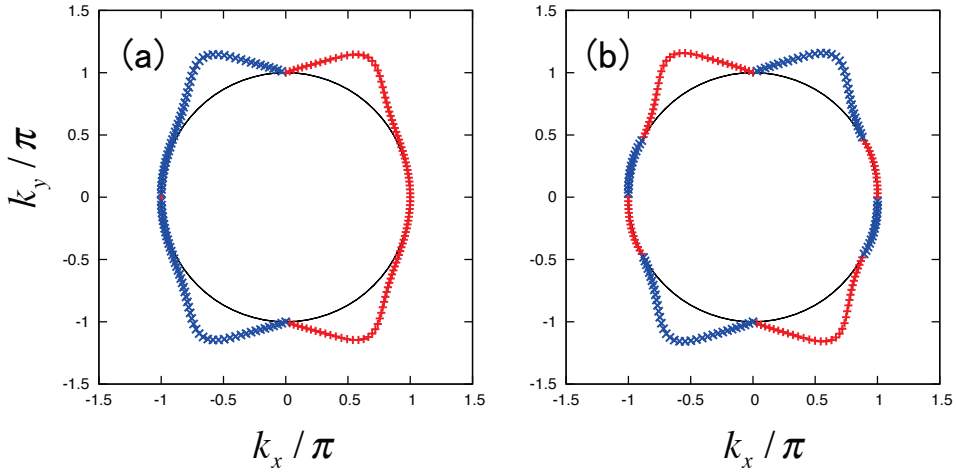

Figure 3. The superconducting gap function for (a) electrons with no vorticity and (b) Dirac fermions. For the pairing interaction (4) we take $\mathbf{q} = (\pi, 0)$ and $\lambda = 0.2$. The thin solid line is the Fermi surface. The thick red and blue lines show the gap function $\Delta_{\mathbf{k}}$. The red lines are for $\Delta_{\mathbf{k}} > 0$ and the blue lines are for $\Delta_{\mathbf{k}} < 0$. The distance in the radial direction between the thick lines and the thin line represents the magnitude of $|\Delta_{\mathbf{k}}|$ in an arbitrary scale.

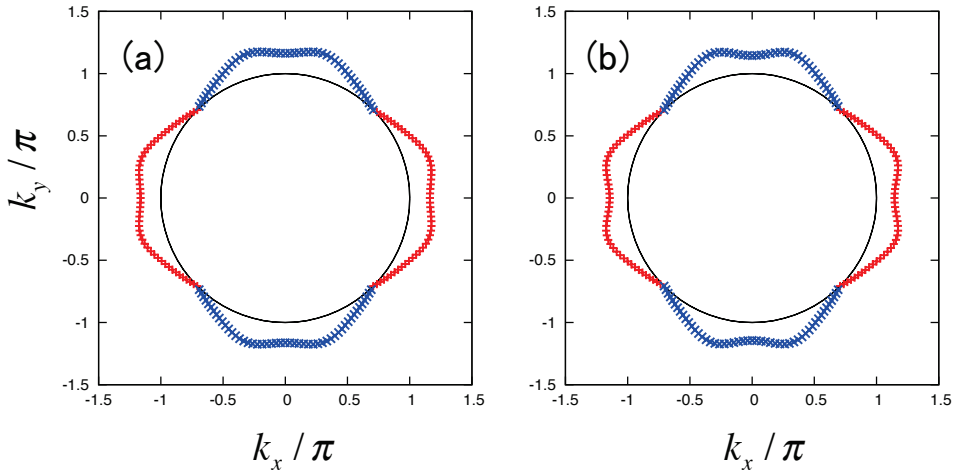

Figure 4. The superconducting gap function for (a) electrons with no vorticity and (b) Dirac fermions. For the pairing interaction (4) we take $\mathbf{q} = (\pi, \pi)$ and $\lambda = 0.2$. The definition of the thin line and the thick lines are the same as that in Fig. 3.

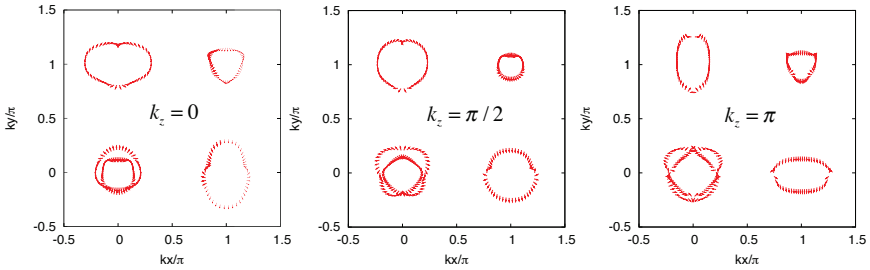

Figure 5. The pseudospin configuration on the Fermi surfaces of iron-based superconductors for different k_z. The change of the pseudospin configuration mainly comes from the change of the shape of the Fermi surfaces. Vorticity itself does not depend on k_z.

Fig. 7(b). The normal electron case is Fig. 6(a) and Fig. 7(a). Contrary to the Dirac fermion case we do not find qualitative difference for the case of $\mathbf{q} = (\pi, 0)$ between the vorticity two case and the normal electron case. Since vorticity is two, there is no suppression of the pairing matrix elements. The chiralities of $\mathbf{k}$ and $-\mathbf{k}$ on the same Fermi surface are equivalent, and so there is no suppression of the matrix elements.

Contrary to the case of $\mathbf{q} = (\pi, 0)$, there is clear qualitative difference for the case of $\mathbf{q} = (\pi, \pi)$. For the case of vorticity zero there are the nodal structures on the electron Fermi surface around $(\pi, 0)$ and $(0, \pi)$. These nodal structure disappear for the case of vorticity two. On the other hand, there are no nodal structure on hole Fermi surfaces around $(0, 0)$ and (π, π) for the case of vorticity zero. However, nodal structures appear on those hole Fermi surfaces for the case of vorticity two. These qualitative difference is associated with the chirality effect.

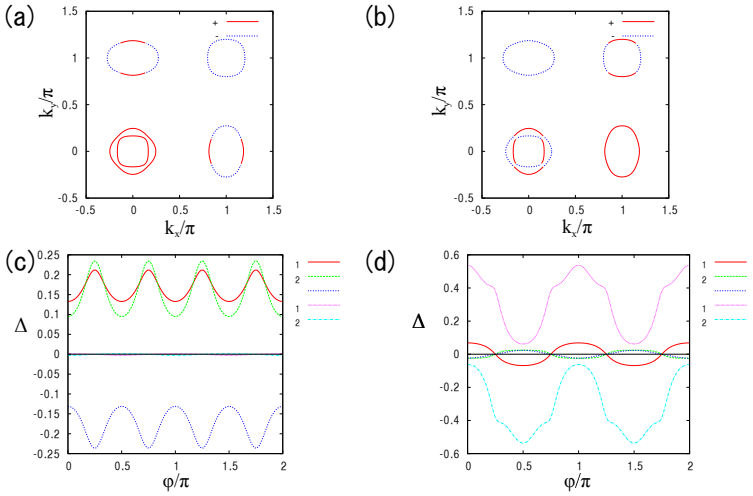

Figure 6. The superconducting gap function at $k_z = 0$ with $\mathbf{q} = (\pi, 0)$ for vorticity zero, (a) and (c) and for vorticity two, (b) and (d). The average electron number at Fe sites is 5.9, that is, a hole doped system. In (a) and (b), the sign of the gap functions on each Fermi surface is shown. The amplitude of the gap function on each Fermi surface is shown in (c) and (d). The inner and outer hole Fermi surfaces at Γ point are denoted by α_1 and α_2, respectively. The hole Fermi surface at (π, π) is denoted by γ and the electron Fermi surfaces at $(\pi, 0)$ and $(0, \pi)$ are denoted by β_1 and β_2, respectively.

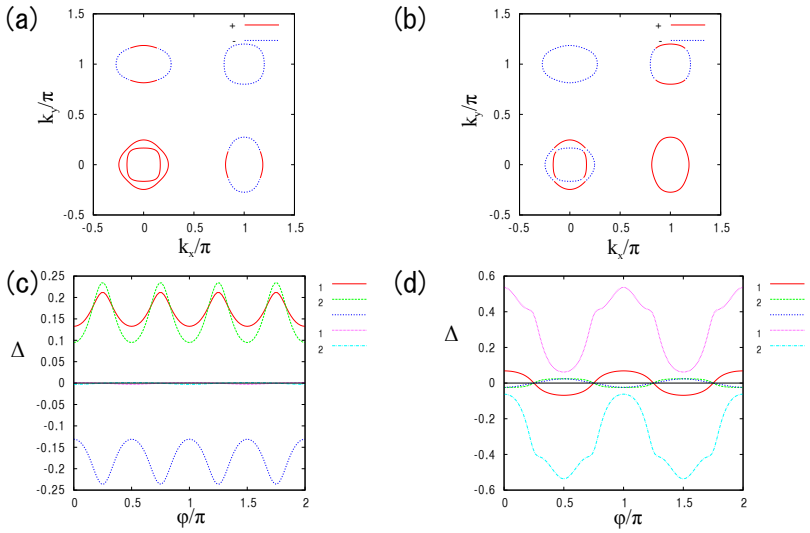

Figure 7. The superconducting gap function at $k_z = 0$ with $\mathbf{q} = (\pi, \pi)$ for vorticity zero, (a) and (c) and for vorticity two, (b) and (d). The average electron number at Fe sites is 5.9. In (a) and (b), the sign of the gap functions at each Fermi surface is shown. The amplitude of the gap function on each Fermi surface is shown in (c) and (d).

The gap function of the three dimensional Fermi surfaces is shown in Fig. 8. The difference between vorticity zero and vorticity two is clearly seen for the case of $\mathbf{q} = (\pi, \pi)$ ((c) and (d)). For the case of $\mathbf{q} = (\pi, 0)$ ((a) and (b)) there is some quantitative difference but no qualitative difference.

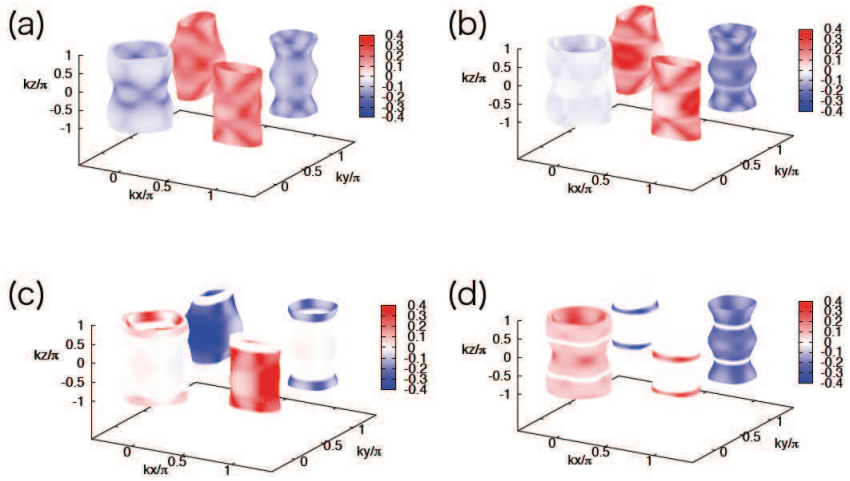

Figure 8. The gap function of the three dimensional Fermi surfaces. for vorticity zero, (a) and (c) and for vorticity two, (b) and (d). The average electron number at Fe sites is 5.9. The wave vector $\mathbf{q}$ of the pairing interaction is $\mathbf{q} = (\pi, 0)$ for (a) and (b) and $\mathbf{q} = (\pi, \pi)$ for (c) and (d).

5. Summary

To summarize, we have studied chirality effect on superconducting states of electrons characterized by chirality. Because of the chirality effect the superconducting gap function has a nodal structure. This node creation mechanism depends on the pairing interaction wave vector $\mathbf{q}$ and vorticity of the electrons. For the case of vorticity one, the node creation mechanism plays an important role for $\mathbf{q} = (\pi, 0)$. For the case of vorticity two, which corresponds to the case of iron-based superconductors, the node creation mechanism plays an important role for $\mathbf{q} = (\pi, \pi)$.

Although this node creation mechanism itself is interesting, the electrons with vorticity would be useful to detect the pairing symmetry of a superconducting state by a proximity effect. We will consider this problem in a future publication.

Acknowledgments

I would like to thank T. Tohyama and E. Kaneshita for helpful discussions. This work was supported by a Grant-in-Aid for Scientific Research (A) (No. 24244053), (C) (No. 24540370), and (B) (No. 25287089), from the Ministry of Education, Culture, Sports, Science, and Technology, Japan.

References

[1] Novoselov K S, Geim A K, Morozov S V, Jiang D, Katsnelson M I, Grigorieva I V, Dubonos S V and Firsov A A 2005 *Nature* **438** 197
[2] Zhang Y, Tan Y W, Stormer H L and Kim P 2005 *Nature* **438** 201
[3] Geim A K and Novoselov K S 2007 *Nat. Mater.* **6** 183–191
[4] Ando T, Nakanishi T and Saito R 1998 *J. Phys. Soc. Jpn.* **67** 2857
[5] Ran Y, Wang F, Zhai H, Vishwanath A and Lee D H 2009 *Phys. Rev. B* **79** 014505
[6] Richard P, Nakayama K, Sato T, Neupane M, Xu Y M, Bowen J H, Chen G F, Luo J L, Wang N L, Dai X, Fang Z, Ding H and Takahashi T 2010 *Phys. Rev. Lett.* **104** 137001
[7] Morinari T, Kaneshita E and Tohyama T 2010 *Phys. Rev. Lett.* **105** 037203
[8] Kuroki K, Onari S, Arita R, Usui H, Tanaka Y, Kontani H and Aoki H 2008 *Phys. Rev. Lett.* **101** 087004
[9] Graser S, Kemper A F, Maier T A, Cheng H P, Hirschfeld P J and Scalapino D J 2010 *Phys. Rev. B* **81** 214503